## General Disclaimer

## One or more of the Following Statements may affect this Document

- This document has been reproduced from the best copy furnished by the organizational source. It is being released in the interest of making available as much information as possible.

- This document may contain data, which exceeds the sheet parameters. It was furnished in this condition by the organizational source and is the best copy available.

- This document may contain tone-on-tone or color graphs, charts and/or pictures, which have been reproduced in black and white.

- This document is paginated as submitted by the original source.

- Portions of this document are not fully legible due to the historical nature of some of the material. However, it is the best reproduction available from the original submission.

28415-HJ07-R0-00

CR 151736

# EQUATIONS FOR CALCULATING ORBITER SURFACE EROSION AND BREAKAGE RATES IN IUS AND SSUS SRM EXHAUST PLUMES

6 JUNE 1978



Prepared for

National Aeronautics and Space Administration
Lyndon B. Johnson Space Center

Contract NAS 9-~~14273~~
14723


Prepared by

S. W. Wilson
Systems Engineering and Analysis Department

TRW
DEFENSE AND SPACE SYSTEMS GROUP

Houston, Texas

# EQUATIONS FOR CALCULATING ORBITER SURFACE EROSION AND BREAKAGE RATES IN IUS AND SSUS SRM EXHAUST PLUMES

6 JUNE 1978

Prepared for
National Aeronautics and Space Administration
Lyndon B. Johnson Space Center
Contract NAS 9-~~14273~~
14723

Prepared by
S. W. Wilson
Systems Engineering and Analysis Department

TRW
DEFENSE AND SPACE SYSTEMS GROUP
Houston, Texas

# EQUATIONS FOR CALCULATING ORBITER SURFACE EROSION AND BREAKAGE RATES IN IUS AND SSUS SRM EXHAUST PLUMES

6 JUNE 1978

Prepared for
NATIONAL AERONAUTICS AND SPACE ADMINISTRATION
L/NDON B. JOHNSON SPACE CENTER

Contract NAS 9-~~14273~~

Prepared by S.W. Wilson

S. W. Wilson, Manager
Shuttle/IUS Proximity
Operations Software Project

Approved by D K Phillips

D. K. Phillips, Manager
Systems Engineering and
Analysis Department

Systems Engineering and Analysis Department

TRW
DEFENSE AND SPACE SYSTEMS GROUP

Houston, Texas

## ABSTRACT

Reference 1 contains equations and coefficients for calculating the flux of solid particles in the exhaust plumes of IUS and SSUS solid rocket motors (SRM's). It also contains equations for calculating surface erosion and breakage rates for Orbiter windows and thermal protection tiles that are exposed to the particle flux. The equations, as written in Reference 1, are directly applicable only when the SRM and the Orbiter are both stationary in some inertial frame. This report describes the equation modifications that are required to account for the independent motions of the Orbiter and the SRM, such as will result during an on-orbit SRM firing. It is intended to incorporate the modified equations in a version of the HP-9825A High Fidelity Relative Motion Program (HFRMP) that is being configured for detailed analysis of SRM damage effects.

TABLE OF CONTENTS

## LIST OF TABLES



## LIST OF FIGURES

## SYMBOLS AND ACRONYMS

| | |
|---|---|
| A, B, C | Polynomial coefficients of $P(\theta)$ |
| a | Thrust acceleration, $cm/sec^2$ |
| D | Particle diameter, cm |
| E | Particle energy factor, $cm^5/sec^2$ |
| f | Mass fraction of a particle family, relative to total mass of aluminum oxide particles |
| G | Cratering constant $(sec/cm)^{2/3}$ |
| IUS | Inertial Upper Stage |
| J | Maximum value of subscript j |
| K | Maximum value of subscript k |
| $\dot{M}$ | Propellant mass flow rate (gm/sec) |
| $P(\theta)$ | Plume shape factor |
| R | $V(\tau-t)$, cm |
| $\bar{r}$ | SRM position vector with respect to Orbiter, cm |
| $\hat{r}$ | $\bar{r}/r$ |
| r | $(\bar{r}\cdot\bar{r})^{1/2}$, cm |
| SRM | Solid rocket motor |
| SSUS | Spinning Solid Upper Stage |
| $\hat{T}$ | SRM thrust unit vector |
| t | Time (of particle ejection), sec |
| $\bar{V}$ | Particle ejection velocity with respect to SRM, cm/sec |
| V | $(\bar{V}\cdot\bar{V})^{1/2}$, cm/sec |
| $\bar{v}$ | SRM velocity vector with respect to Orbiter, cm/sec |
| v | $(\bar{v}\cdot\bar{v})^{1/2}$, cm/sec |
| $\bar{W}$ | Particle velocity vector with respect to Orbiter, cm/sec |
| W | $(\bar{W}\cdot\bar{W})^{1/2}$, cm/sec |

| | |
|---|---|
| $\beta$ | Number of breaks per unit of surface area, $cm^{-2}$ |
| $\varepsilon$ | Pitted fraction of surface area (erosion) |
| $\theta$ | Particle streamline angle (angle of ejection with respect to SRM exhaust centerline) |
| $\rho$ | Mass density, $gm/cm^3$ |
| $\tau$ | Time (of particle impact), sec |

SUBSCRIPTS

| | |
|---|---|
| a | Greater root of Equation (20) |
| b | Lesser root of Equation (20) |
| i | Function of particle diameter |
| j | Function of particle ejection time |
| k | Function of particle impact time |

# 1. INTRODUCTION

According to Reference 1, 34% of the mass ejected from the SRM consists of aluminum oxide particles having diameters in the range of .0178 to 10 microns. In addition, approximately 0.25% of the mass consists of carbon that is eroded from the SRM nozzle and which is assumed to be ejected also in the form of particles with diameters ranging between 17.8 and 1000 microns. Damage inflicted to Orbiter windows and thermal protection tiles by these particles is classified either as erosion or as breakage.

In the case of a thermal protection tile, a break represents a penetration of its silicon surface. A window break represents the formation of a pit of such a depth (46 microns or more) that subsequent thermal stress experienced during atmospheric entry will cause crack propagation in the window. The formation of pits that are too shallow to penetrate the silicon surface of a tile or to induce crack propagation in a window is classified as erosion damage. Erosion ($\varepsilon$) is measured in terms of the fraction of the surface area that is affected by these shallower pits. Breakage ($\beta$) is measured in terms of the number of breaks per unit of surface area. Proposed limits for breakage and erosion damage are contained in Reference 2.

## 2. EQUATIONS FOR STATIONARY ORBITER AND SRM

For the purpose of modeling the SRM exhaust plume, the total population of ejected particles is divided into 20 discrete families (12 families of aluminum oxide particles and 8 families of carbon particles). Each family i (i = 1, 2, ...., 20) is assumed to consist of particles having a uniform diameter $D_i$ which are ejected with a fixed speed $V_i$ relative to the SRM. According to Reference 1, the mass flux ($\dot{m}_i/dS$) of particles from the $i^{th}$ family that impinge on a surface element dS normal to the particle streamline is given by the equation

$$\rho_i V_i = 0.34\ \dot{M}\ f_i P_i(\theta) / (4\pi R^2)\ , \qquad (1)$$

where $\rho_i$ is the mass density of the particle family at the point of impact. The symbol $\dot{M}$ represents the total SRM propellant mass flow rate, $f_i$ is the mass ratio for the $i^{th}$ particle family with respect to the total mass of aluminum oxide particles, R is the distance between the SRM and the surface element, $\theta$ is the angle subtended by the SRM exhaust plume centerline and the particle streamline (velocity vector), and

$$P_i(\theta) = A_i\theta^2 + B_i\theta + C_i \qquad (2)$$

is a plume "shape factor" defined by a polynomial curve fit.

Equation (1) is strictly valid only when, as illustrated in Figure 1, both the SRM and the surface element are stationary in some frame wherein the individual particle velocity vectors are constant. In such a frame, the surface erosion rate for the $i^{th}$ particle family is given by

$$\dot{\varepsilon}_i = 1.5\ G_i^2\ \rho_i\ V_i^{7/3}\ /D_i\ , \qquad (3)$$

where $G_i$ is the "cratering constant" for the family in question. The breakage rate is given by

$$(\text{if } E \leq E^*)\text{: } \dot{\beta}_i = 0 \qquad (4a)$$

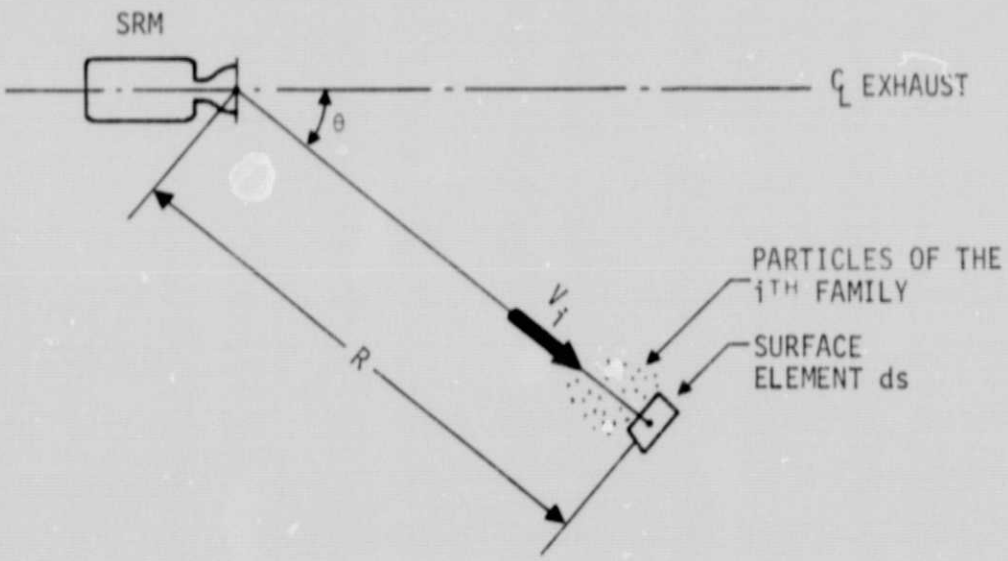


Figure 1. Particle Flux Illustration for Stationary SRM and Surface Element

or

$$(\text{if } E > E^*): \dot{\beta}_i = 0.95\, \rho_i V_i / D_i^3 , \tag{4b}$$

where E is an energy factor given by

$$E = D_i^3 V_i^2 , \tag{5}$$

and where the value of $E^*$, as indicated in Table 1, depends on the type of surface that is being impinged. Coefficients that define the characteristics of the various particle families in the plume of the large IUS motor are given in Table 2.

TABLE 1

CRITICAL ENERGY FACTORS

| SURFACE TYPE | $E^*$ ($cm^5/sec^2$) |
|---|---|
| Window | $1.85 \times 10^3$ |
| Low-Temperature Tile | $1.56 \times 10^5$ |
| High-Temperature Tile | $1.25 \times 10^6$ |

| | i | D (CM) | f | V (CM/SEC) | $G^{\frac{1}{6}}$ $\left(\frac{cm^5 sec^4}{gm^3}\right)^{\frac{1}{6}}$ | REGION A ($RAD^{-2}$) | REGION B ($RAD^{-1}$) |
|---|---|---|---|---|---|---|---|
| ALUMINUM OXIDE PARTICLES | 1 | $0.0178 \times 10^{-4}$ | .000017 | $3.719 \times 10^{5}$ | $2.78 \times 10^{-4}$ | 0 | 0 |
| | 2 | 0.0316 | .00061 | 3.719 | $2.78 \times 10^{-4}$ | 0 | 0 |
| | 3 | 0.0562 | .012 | 3.719 | | 0 | 0 |
| | 4 | 0.100 | .12 | 3.719 | | -12.7 | -.634 |
| | 5 | 0.178 | .27 | 3.713 | | -11.1 | 0 |
| | 6 | 0.316 | .068 | 3.688 | | -3.02 | -.737 |
| | 7 | 0.562 | .086 | 3.658 | | -1.05 | -.572 |
| | 8 | 1.00 | .19 | 3.612 | | -4.09 | .642 |
| | 9 | 1.78 | .19 | 3.530 | $2.78 \times 10^{-4}$ | 4.40 | .230 |
| | 10 | 3.16 | .054 | 3.406 | $9.75 \times 10^{-4}$ | 19.6 | 0 |
| | 11 | 5.62 | .0027 | 3.240 | $9.75 \times 10^{-4}$ | 0 | 0 |
| | 12 | 10.0 | .000012 | 3.002 | $9.75 \times 10^{-4}$ | 0 | 0 |
| CARBON PARTICLES | 13 | 17.8 | .0068 | 2.658 | 0 | 0 | 0 |
| | 14 | 31.6 | | 2.560 | | | |
| | 15 | 56.2 | | 2.057 | | | |
| | 16 | 100. | | 1.600 | | | |
| | 17 | 178. | | 1.219 | | | |
| | 18 | 316. | | .920 | | | |
| | 19 | 562. | | .686 | | | |
| | 20 | 1000. $\times 10^{-4}$ | .0068 | $.494 \times 10^{5}$ | 0 | 0 | 0 |

NOTES:

FOLDOUT FRAME

Table 2. SRM Plume Particle Data for Large IUS Motor (From Reference 1)

| P(θ) COEFFICIENTS | | | | | | | | | | | |
|---|---|---|---|---|---|---|---|---|---|---|---|
| REGION I | | | (1) | REGION II | | | (2) | REGION III | | | (3) |
| A ($RAD^{-2}$) | B ($RAD^{-1}$) | C | $\theta_{max}$ (DEG) | A ($RAD^{-2}$) | B ($RAD^{-1}$) | C | $\theta_{max}$ (DEG) | A ($RAD^{-2}$) | B ($RAD^{-1}$) | C | $\theta_{max}$ (DEG) |
| 0 | 0 | 0 | 0.0 | -9.78 | -1.56 | 10.2 | 20.0 | -7.05 | -5.17 | 11.1 | 54.0 |
| 0 | 0 | 0 | 0.0 | -9.78 | -1.56 | 10.2 | 20.0 | -7.05 | -5.17 | 11.1 | 54.0 |
| 0 | 0 | 0 | 0.0 | -8.52 | -1.78 | 10.3 | 20.0 | -6.23 | -6.92 | 11.8 | 53.5 |
| -12.7 | -.634 | 10.6 | 12.0 | -72.7 | 35.5 | 5.68 | 22.0 | -7.11 | -7.26 | 12.4 | 52.0 |
| -11.1 | 0 | 10.8 | 12.0 | -44.5 | 18.6 | 8.40 | 22.0 | -6.89 | -9.10 | 13.5 | 50.0 |
| -3.02 | -.737 | 11.0 | 10.0 | -33.2 | 12.2 | 9.68 | 18.0 | -12.0 | -4.86 | 12.9 | 47.5 |
| -1.05 | -.572 | 11.6 | 9.0 | -58.4 | 24.0 | 9.14 | 16.0 | -20.9 | 1.42 | 12.5 | 44.0 |
| -4.09 | .642 | 12.4 | 9.0 | -91.8 | 39.5 | 8.51 | 16.0 | -26.4 | 3.30 | 13.5 | 39.5 |
| 4.40 | .230 | 14.4 | 9.0 | -115. | 49.8 | 9.66 | 16.0 | -50.3 | 19.0 | 13.1 | 33.5 |
| 19.6 | 0 | 19.1 | 8.0 | -118. | 48.1 | 15.1 | 16.0 | -28.6 | 2.49 | 20.9 | 27.0 |
| 0 | 0 | 0 | 0.0 | 276. | -12.5 | 25.9 | 11.0 | -614. | 316. | -4.32 | 20.0 |
| 0 | 0 | 0 | 0.0 | 856. | -8.97 | 46.9 | 9.0 | -514. | 367. | 21.6 | 14.0 |
| 0 | 0 | 0 | 0.0 | 0 | 0 | 0 | 21.4 | -2000. | 1380. | -165. | 28.6 |
| ↕ | ↕ | ↕ | ↕ | ↕ | ↕ | ↕ | 19.7 | -1790. | 1190. | -147. | 28.2 |
| | | | | | | | 18.3 | -1200. | 704. | -53.6 | 27.8 |
| | | | | | | | 17.0 | -923. | 484. | -15.6 | 27.4 |
| | | | | | | | 16.3 | -731. | 320. | 16.2 | 27.0 |
| | | | | | | | 15.8 | -599. | 198. | 41.8 | 26.6 |
| | | | | | | | 15.4 | -531. | 110. | 63.5 | 26.0 |
| 0 | 0 | 0 | 0.0 | 0 | 0 | 0 | 15.1 | -490. | 40.6 | 82.5 | 25.5 |

NOTES: (1) $\theta_{min\ I} = 0$ (2) $\theta_{min\ II} = \theta_{max\ I}$ (3) $\theta_{min\ III} = \theta_{max\ II}$

FOLDOUT FRAME 2

ORIGINAL PAGE IS OF POOR QUALITY

## 3. EQUATIONS FOR NON-STATIONARY ORBITER AND SRM

In order to calculate the surface erosion and breakage rates that attend an actual on-orbit SRM firing, it is necessary to account for the facts that (1) the Orbiter and the SRM are not stationary in any inertial frame, (2) a finite time interval elapses between the ejection of a particle from the SRM and its impact on an Orbiter surface, and (3) the SRM propellant mass flow rate varies with time, as illustrated in Figure 2 for the large IUS motor.

We assume that the SRM's thrust unit vector $\hat{T}$ and its Orbiter-relative position vector $\overline{r}$ and velocity vector $\overline{v}$, all measured in some convenient non-rotating reference frame, are available (along with the mass flow rate $\dot{M}$) as tabulated functions of the particle ejection time t. Let the subscript $j = 1, 2, 3, \ldots, J$ be an index to designate a particular tabulated value of t. We assume that the time t is measured from SRM ignition. We also assume the input data table is arranged such that $t_1 = 0$ and $t_J = \Delta t_{BURN}$ (where $\Delta t_{BURN}$ is the time required to consume all of the SRM propellant), and such that $t_j$ increases monotonically with j. (It is intended to construct this data table during a prior execution of the HFRMP trajectory integration routine; however, any suitable powered-flight trajectory integration program could be used.)

Our goal is to tabulate, for each family i, particle trajectory data that will permit the calculation of erosion and breakage rates as functions of the particle impact time $\tau$. Let the subscript $k = 1, 2, 3, \ldots, K$ be an index to designate a particular tabulated value of $\tau$. If the output data tables are arranged such that (for any value of i) $\tau_{ik}$ increases monotonically with k, then it will be a relatively simple matter to calculate the total erosion and breakage that results from the SRM firing, by numerically integrating the rates with respect to $\tau$ and summing over all values of i.

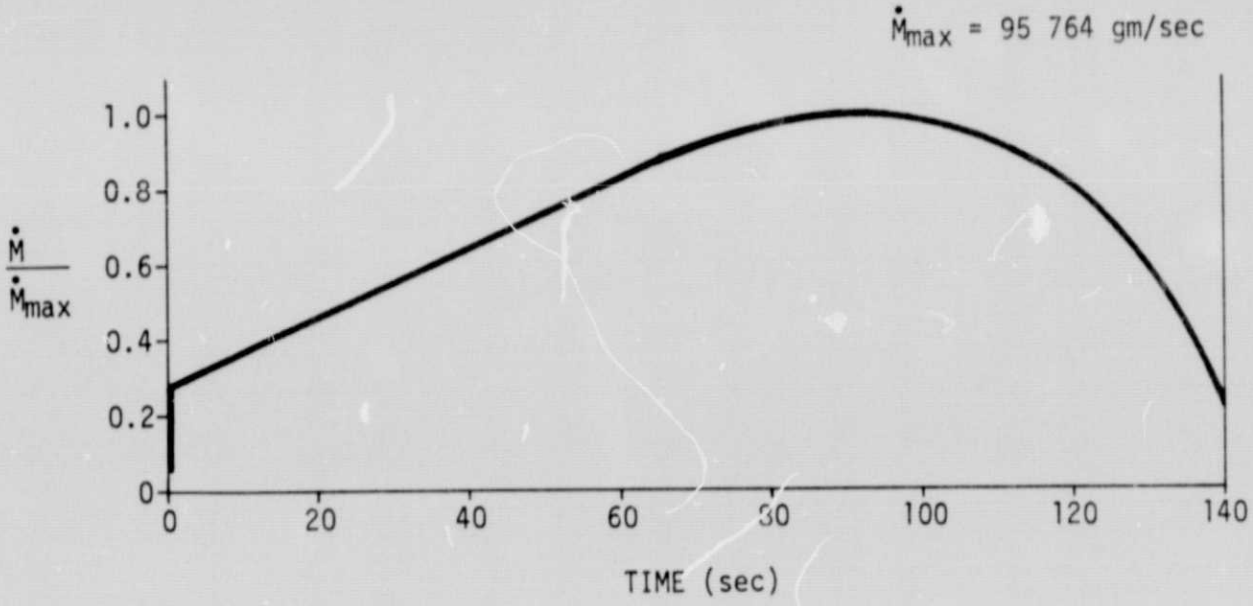


Figure 2. Mass Flow Rate Variation (Large IUS Motor)

The calculations will be simplified by assuming that, between the times of ejection and impact at least, the velocity of a given particle with respect to the Orbiter is constant in the non-rotating frame. At the orbit altitudes of interest (on the order of 150 nautical miles), such an approximation is reasonably accurate for particle flight times up to about five minutes, provided no thrust is being applied to the Orbiter. With this simplification, the particle velocity with respect to the Orbiter at impact time is given by the equation

$$\overline{W}_{ik} = \overline{v}_j + \overline{V}_{ik} \ , \tag{6}$$

where $\overline{V}_{ik}$ is the velocity of the particle with respect to the SRM at ejection time. The particle impact time is given by the equation

$$\tau_{ik} = t_j + r_j/W_{ik} \ , \tag{7}$$

where

$$r_j = (\overline{r}_j \cdot \overline{r}_j)^{1/2} \tag{8}$$

and

$$W_{ik} = (\overline{W}_{ik} \cdot \overline{W}_{ik})^{1/2} \ . \tag{9}$$

## 3.1 EROSION AND BREAKAGE RATES

As yet, we have no way of evaluating $\overline{W}_{ik}$ for an impinging particle because, although the magnitude of $\overline{V}_{ik}$ is known to be $V_i$ (a function of particle size alone), its direction has not been determined. This problem will be addressed shortly. For the time being, let us assume that $\overline{W}_{ik}$ is known, and examine the modified equations for erosion and breakage rates.

These are obtained by substituting $W_{ik}$ for $V_i$ and $\rho_{ik}$ for $\rho_i$ in Equation (3) through (5), which yields

$$\overset{\nabla}{\varepsilon}_{ik} = 1.5\ G_i^2\ \rho_{ik}\ W_{ik}^{7/3} / D_i \tag{10}$$

and

$$(\text{if } E_{ik} \leq E^*) : \overset{\nabla}{\beta}_{ik} = 0 \tag{11a}$$

or

$$(\text{if } E_{ik} > E^*) : \overset{\nabla}{\beta}_{ik} = 0.95\ \rho_{ik} W_{ik} / D_i^3\ , \tag{11b}$$

where

$$E_{ik} = D_i^3\ W_{ik}^2\ , \tag{12}$$

and where the superposition of an inverted triangle over a symbol designates the derivative of the indicated variable with respect to $\tau$. Thus, for instance, $\overset{\nabla}{\varepsilon} \equiv d\varepsilon/d\tau$ in the same fashion that $\dot{\varepsilon} \equiv d\varepsilon/dt$.

The mass density appearing in Equation (10) and (11b) can be calculated from the equation

$$\rho_{ik} = \frac{0.34\ \dot{M}_j f_i P_i(\theta_{ik}) W_{ik}^2}{4\pi\ r_j^2\ V_i^3}\ . \tag{13}$$

Equation (13 results from Equations (1) and (7) when it is recognized that, in the general case, the variable R which appears in (1) represents nothing more or less than the product of $V_i$ and the particle flight time. An expression for the particle ejection angle $\theta_{ik}$, which appears in Equation (13), will be presented after solving for $\overline{W}_{ik}$ in the next section.

Equations (10) through (12) indicate that erosion and breakage rates (at least for a surface normal to the relative velocity vector of the impinging particles) can be integrated if only three particle trajectory variables ($\tau_{ik}$, $\rho_{ik}$, and $W_{ik}$) are included in the output data tables. However, since it is considered desirable to know the direction as well as the magnitude of the particle flux, it is intended to tabulate the three Cartesian components of $\overline{W}_{ik}$ rather than just its magnitude $W_{ik}$. Given the orientation of the Orbiter relative to the non-rotating frame, this will permit (among other things) the possible use of more sophisticated erosion and breakage rate equations that would account for the effects of particle incidence angle variations on specific Orbiter surfaces.

## 3.2 CALCULATION OF PARTICLE VELOCITY RELATIVE TO ORBITER

With the simplifying assumption that has been made, the direction of $\overline{W}_{ik}$ must be opposite to that of $\overline{r}_j$ if the particle in question is to strike the Orbiter. Therefore, we can write

$$\overline{W}_{ik} = - \hat{r}_j \, W_{ik}, \tag{14}$$

where

$$\hat{r}_j = \overline{r}_j / r_j \tag{15}$$

Substituting Equation (14) into (6) and rearranging, we obtain

$$- \overline{V}_{ik} = \hat{r}_j \, W_{ik} + \overline{v}_j \, . \tag{16}$$

Noting that $(-\overline{V}_{ik}) \cdot (-\overline{V}_{ik}) = V_i^2$ (a known quantity), we can now write

$$V_i^2 = W_{ik}^2 + v_j^2 + 2 \, W_{ik} \dot{r}_j \, , \tag{17}$$

where

$$v_j^2 = \overline{v}_j \cdot \overline{v}_j \tag{18}$$

and

$$\dot{r}_j = \bar{v}_j \cdot \hat{r}_j . \tag{19}$$

Equation (17) can be rearranged into the standard form of a quadratic in the unknown quantity $W_{ik}$, viz:

$$W_{ik}^2 + (2\dot{r}_j)W_{ik} + (v_j^2 - V_i^2) = 0 , \tag{20}$$

which has the two roots

$$W_{ik_a} = - \dot{r}_j + (\dot{r}_j^2 + V_i^2 - v_j^2)^{1/2} \tag{21a}$$

and

$$W_{ik_b} = - \dot{r}_j - (\dot{r}_j^2 + V_i^2 - v_j^2)^{1/2} . \tag{21b}$$

Any positive real root of Equation (20) represents a particle trajectory that will impinge on the Orbiter, provided the associated ejection angle

$$\theta_{ik} = \cos^{-1} \left[ (\hat{r}_j W_{ik} + \bar{v}_j) \cdot (\hat{T}_j / V_i) \right] \tag{22}$$

is no greater than the limiting streamline angle ($\theta_{\text{max III } i}$ in Table 2) for the particle size under consideration.

Figure 3 is a vector diagram of the solution to Equation (20) for a case in which there are two positive real roots. Geometrically, the real roots of Equation (20) represent the intersections of a line, connecting the positions of the Orbiter and the SRM, with a sphere of radius $V_i$ centered on the head of the Orbiter-relative velocity vector of the SRM. The root is positive when the intersection lies in the direction of the Orbiter (as seen from the SRM), and negative when it lies in the opposite direction. If the line does not intersect the sphere, then the roots of

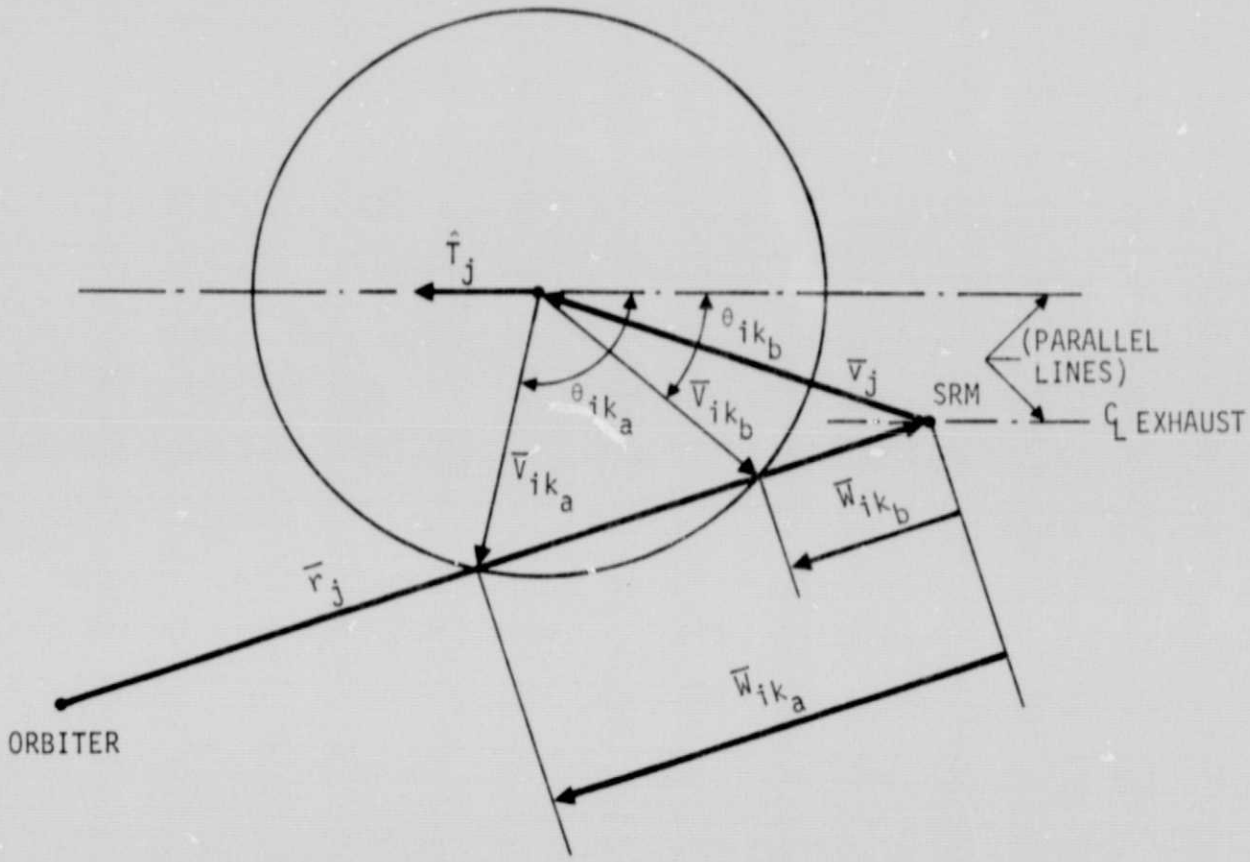


Figure 3. Vector Diagram of Particle Trajectory Solution

Equation (20) are complex (and vice versa). In the more common case where the SRM position lies inside the sphere (i.e., when $v_j < V_i$), there will be one positive and one negative real root.

# 4. CONSTRUCTION OF OUTPUT DATA TABLES

The construction of the desired output array of particle trajectory parameters is complicated by the fact that, at any given time $t_j$, particles of a given size $D_i$ may be ejected from the SRM on two distinctly different trajectories that will both impinge on the Orbiter, but at different impact times. It is easily seen that the K dimension of the output array (where K represents the total number of $\tau_i$ values to be tabulated for a given particle family i) should be at least as large as 2J (where J represents the total number of t values tabulated in the input array). For reasons that will be brought out later, it is actually necessary to set K = 2J+2.

## 4.1 RELATIONSHIP BETWEEN PARTICLE EJECTION AND IMPACT TIMES

To facilitate the subsequent numerical integration of erosion and breakage rates, it is essential to arrange the entries in the output tables in such a manner that, for a given particle diameter $D_i$, the value of $\tau_{ik}$ (where k = 1, 2, 3, ...., K) will increase monotonically with k. With this in mind, it becomes necessary at this point to consider the derivative $\dot{\tau} \equiv d\tau/dt$. This derivative will not be used in the calculation of any output data; we wish only to determine its algebraic sign for the purpose of arranging the values of $\tau_{ik}$ in monotonically increasing order.

Differentiating Equation (7) with respect to t, we obtain

$$\dot{\tau}_{ik} = 1 + \dot{r}_j/W_{ik} - \dot{W}_{ik} r_j/W_{ik}^2 \ , \tag{23}$$

in which $\dot{W}_{ik}$ is, as yet, unknown. Equation (20) is now differentiated, yielding

$$\dot{W}_{ik}(W_{ik} + \dot{r}_j) + \ddot{r}_j W_{ik} + \dot{v}_j v_j = 0 \tag{24}$$

in which two new unknowns ($\ddot{r}_j$ and $\dot{v}_j$) appear. Combining Equations (15) and (19), we can write

$$\dot{r}_j r_j = \bar{v}_j \cdot \bar{r}_j \ , \tag{25}$$

whence (after noting that $\dot{\bar{r}} \equiv \bar{v}$) it follows that

$$\ddot{r}_j r_j = \dot{\bar{v}} \cdot \bar{r}_j + v_j^2 - \dot{r}_j^2 \ , \tag{26}$$

and we can differentiate Equation (18) to obtain

$$\dot{v}_j v_j = \dot{\bar{v}}_j \cdot \bar{v}_j \ . \tag{27}$$

We are left now with a single unknown ($\dot{\bar{v}}_j$) which, for our purpose (considering the thrust magnitude of the SSUS and IUS motors) can be approximated by

$$\dot{\bar{v}}_j = \hat{T}_j a_j \ , \tag{28}$$

where $a_j$ represents the magnitude of the SRM thrust acceleration. Combining Equations (23) through (28), we obtain

$$\dot{\tau}_{ik} = \frac{\left[(W_{ik} + \dot{r}_j)^2 + (v_j^2 - \dot{r}_j^2)\right] W_{ik} + (W_{ik}\bar{r}_j + r_j\bar{v}_j) \cdot \hat{T}_j a_j}{(W_{ik} + \dot{r}_j)\, W_{ik}^2} \ . \tag{29}$$

We note from examination of Equations (15) and (22) that

$$(W_{ik}\bar{r}_j + r_i \bar{v}_j) \cdot \hat{T}_j = r_j V_i \cos \theta_{ik} \ , \tag{30}$$

which can be substituted into Equation (29) to obtain

$$\dot{\tau}_{ik} = \frac{\left[(W_{ik} + \dot{r}_j)^2 + (v_j^2 - \dot{r}_j^2)\right] W_{ik} + a_j r_j V_i \cos \theta_{ik}}{(W_{ik} + \dot{r}_j)\, W_{ik}^2} \ . \tag{31}$$

The limiting streamline angle ($\theta_{\text{max IIIi}}$ in Table 2) is less than 90° for all particles and all SRM's under consideration, therefore cos $\theta_{ik}$ as well as $W_{ik}$ must be positive for any particle trajectory that impinges on the

Orbiter. Furthermore, since $\dot{r}_j$ is a component of $\bar{v}_j$, the quantity $(v_j^2 - \dot{r}_j^2)$ can never be negative. It follows, then, that the numerator on the right side of Equation (31) is always positive. With this in mind, comparing Equations (21a) and (21b) with the denominator on the right side of (31) reveals that

$$\dot{\tau}_{ik_a} > 0 \tag{32a}$$

and

$$\dot{\tau}_{ik_b} < 0, \tag{32b}$$

where $\tau_{ik_a}$ and $\tau_{ik_b}$, respectively, represent impact times for the impinging trajectory sub-families generated by the greater and the smaller root (in an algebraic sense) of Equation (20). If $W_{ik} + \dot{r}_j = 0$, then there are two equal roots, and $\dot{\tau}_{ik_a} = +\infty$ and $\dot{\tau}_{ik_b} = -\infty$.

The preceding facts indicate that in a case where $\tau_i$ is a single-valued function of t (i.e., when there is only one positive root of Equation (20) that produces a value of $\theta_{ik} \leq \theta_{\max\ IIIi}$), the Orbiter-relative mass flux history for the particle family in question will be of the nature indicated in Figure 4. In a case where $\tau_i$ is a double-valued function of t, the mass flux history will be of the nature depicted either in Figure 5 or in Figure 6, depending on whether or not the discriminant of Equation 20 becomes negative before the end of the burn.

If there is an impingement hiatus as depicted in Figure 6, it is necessary at SRM burnout time (i.e., when $j = J$) to make two entries in the output data table for each of the calculated impact times ($\tau_{ik_a}$ and $\tau_{ik_b}$). In each case, in one entry the output variables $\rho_{ik}$ and $\bar{W}_{ik}$ are assigned the values that result from Equations (13) and (14), and in the other entry these variables are assigned values of zero. For this reason, the output data table must be sized to accomodate as many as 2J+2 entries (values of $\tau_i$), rather than only 2J entries.

Figure 4. Impingement History for Single-Valued $\tau_i$

Figure 5. Impingement History for Double-Valued $\tau_i$

Figure 6. Impingement History for Double-Valued $\tau_i$, with Hiatus

## 4.2 COMPUTATIONAL ALGORITHM

The construction of the output tables will be simplified by making a distinction between "literal" entries and "logical" entries. A literal entry corresponds to any actual row of data in the output table. A logical entry corresponds to a row that contains a value of $\tau_{ik} > 0$. (Since time is assumed to be measured from SRM ignition, $\tau_i$ for any impinging particle trajectory must be positive.) During the subsequent numerical integration of erosion and breakage rates, it will be necessary to interpolate between tabulated values of $\tau_{ik}$. The interpolation logic will be defined in such a manner that any non-logical entry (i.e., an entry having a value of $\tau_{ik} \leq 0$) will be ignored.

The following process can be used to arrange logical entries in such a manner that $\tau_{ik}$ increases monotonically with k:

1. Set K = 2J+2 and initialize a three-dimensional array of size 20 x K x 5, by assigning a value of zero to every element of the array. The number 20 represents the number of particle diameters to be considered, K represents the maximum possible number of logical $\tau_i$ values, and 5 represents the number of scalar output variables ($\tau_i$, $\rho_i$, and three components of $\overline{W}_i$ ).

2. For every value of i (i = 1, 2, ...., 20) and every value of j (j = 1, 2, ...., J), evaluate the roots of Equation (20). For every positive real root that produces an ejection angle smaller than the limiting streamline angle:

    a. Set k = j or k = K+1-j, depending on whether Equation (21a) or (21b) was used to calculate the root.

    b. Using Equations (7), (13), and (14), calculate $\tau_{ik}$, $\rho_{ik}$, and $\overline{W}_{ik}$, and store the calculated values in the appropriate elements of the output array.

3. For every i, set $\tau_{i(J+1)} = \tau_{iJ}$ and set $\tau_{i(J+2)} = \tau_{i(J+3)}$.

Figure 7 illustrates this process in the form of a flow chart. The associated interpolation logic is illustrated in Figure 8.

FOLDOUT FRAME

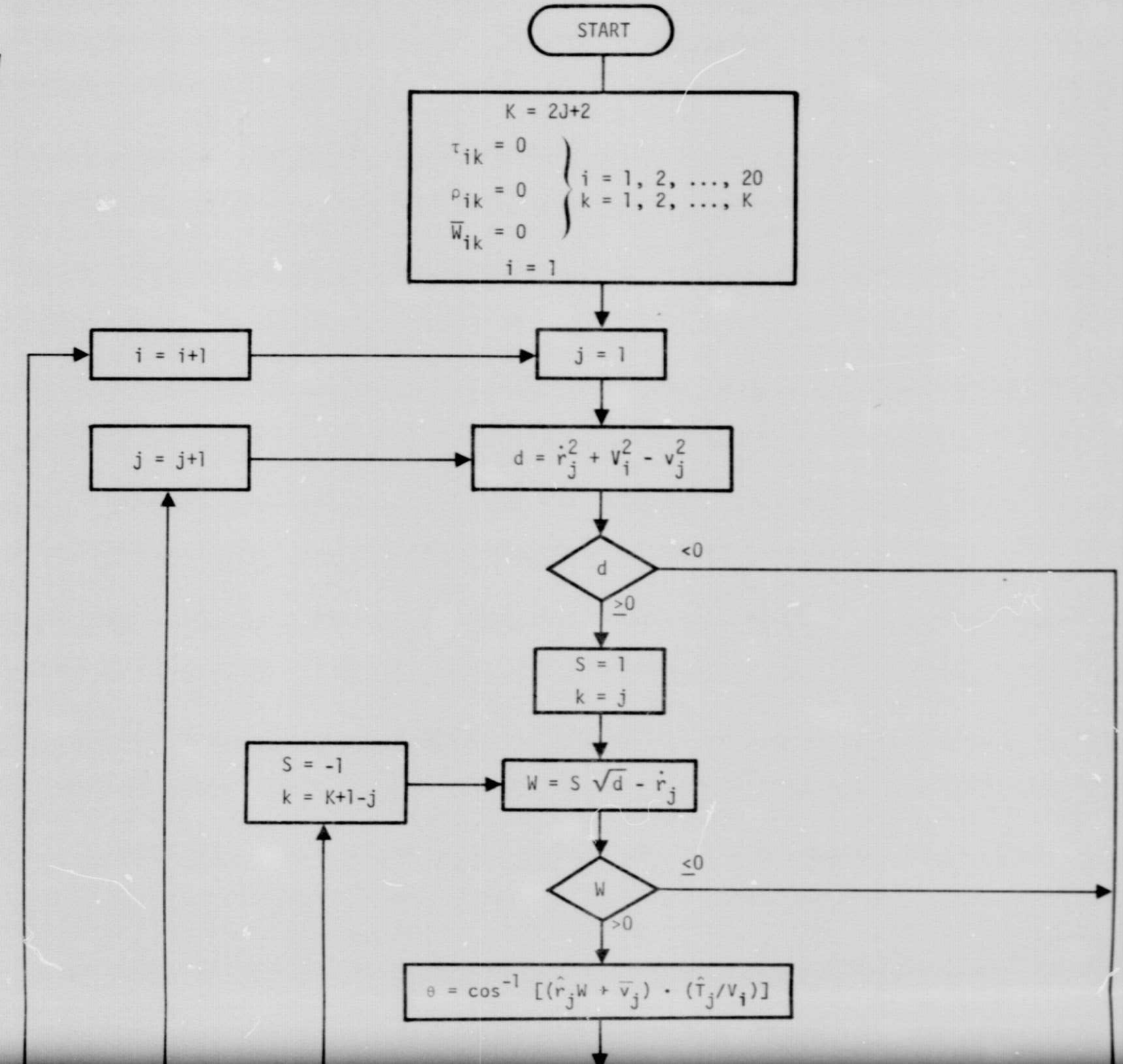

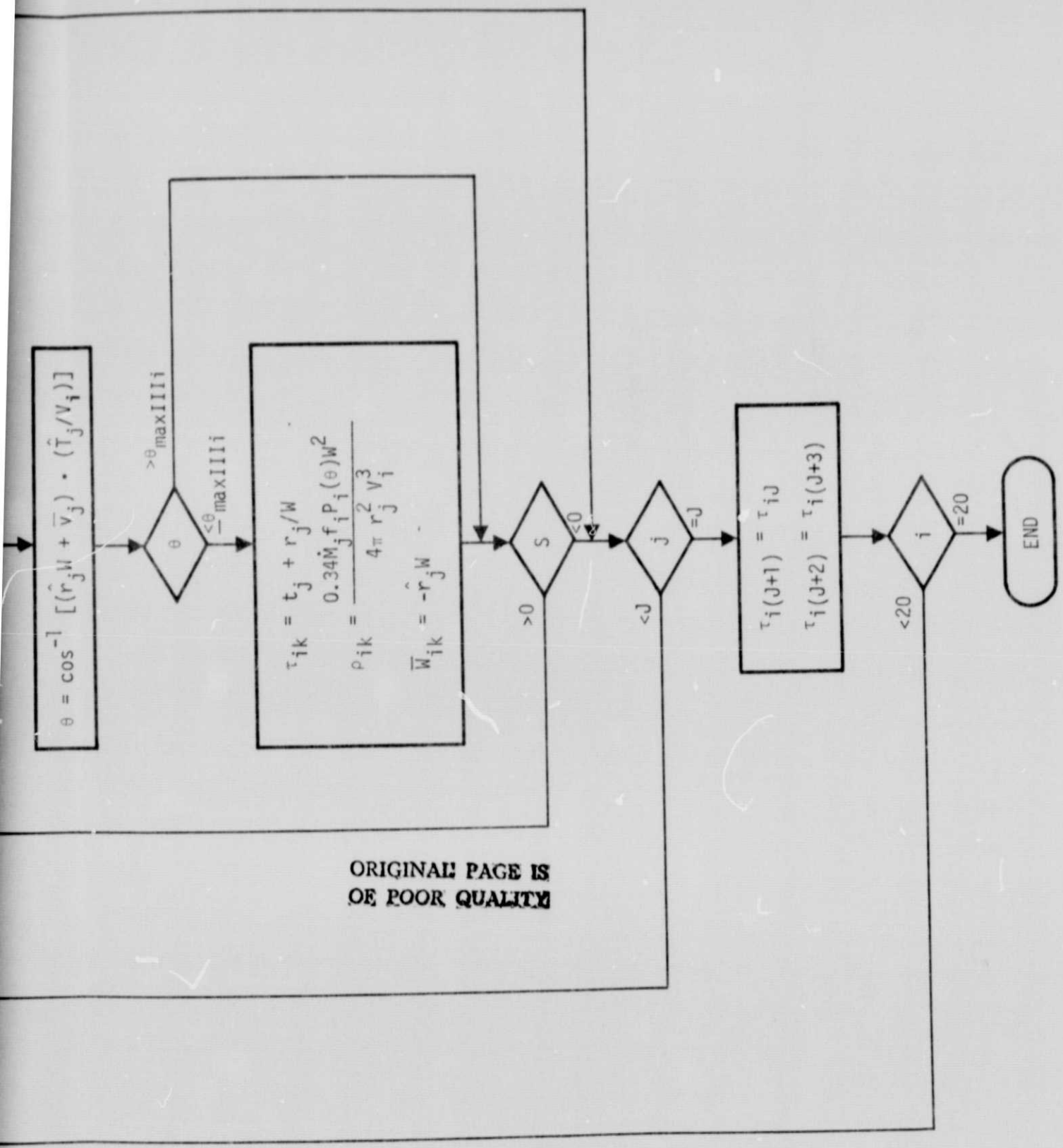


ORIGINAL PAGE IS
OF POOR QUALITY

FOLDOUT FRAME
2

Figure 7. Flow Chart for Construction of Output Data Table

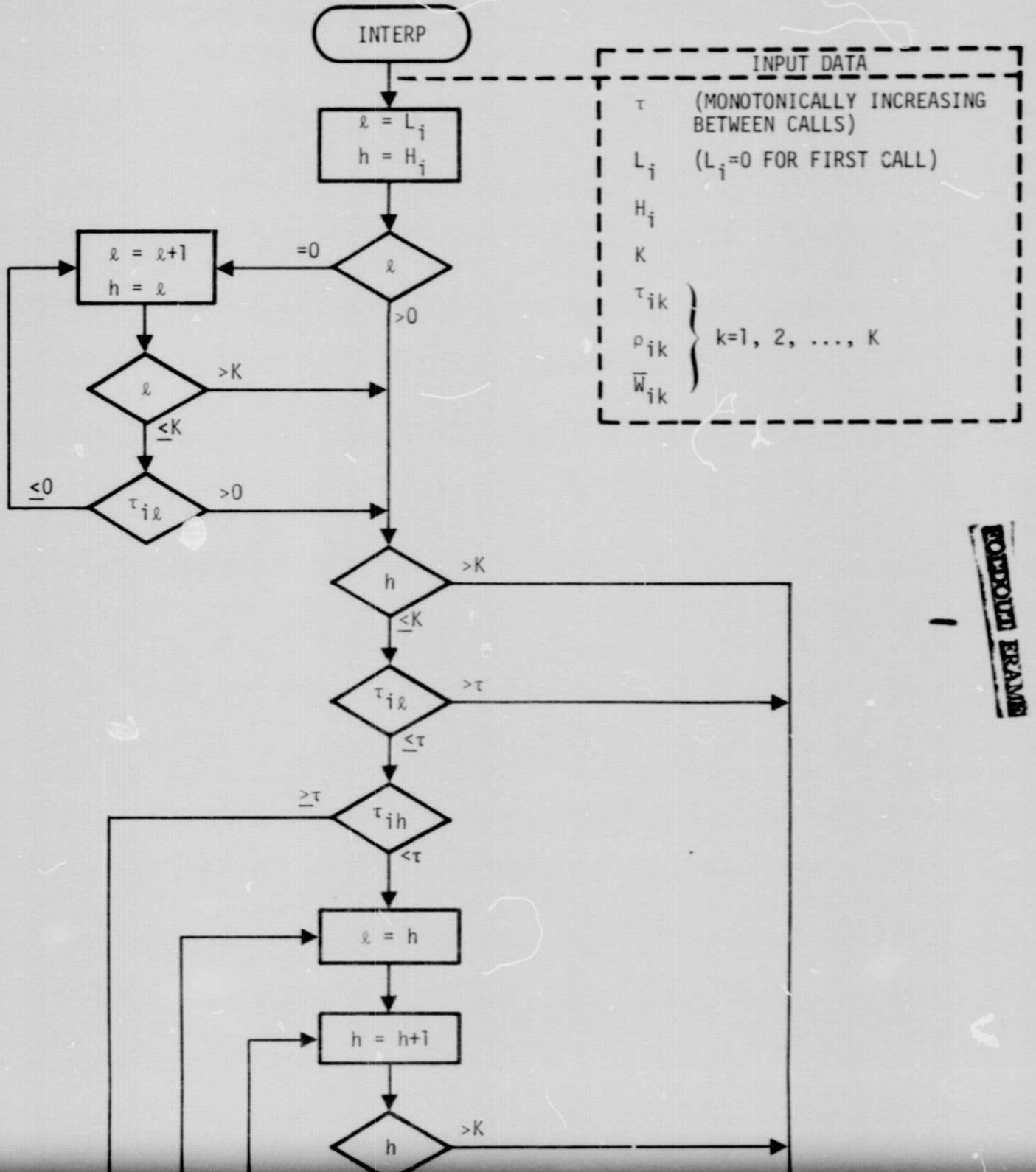

FOLDOUT FRAME 2

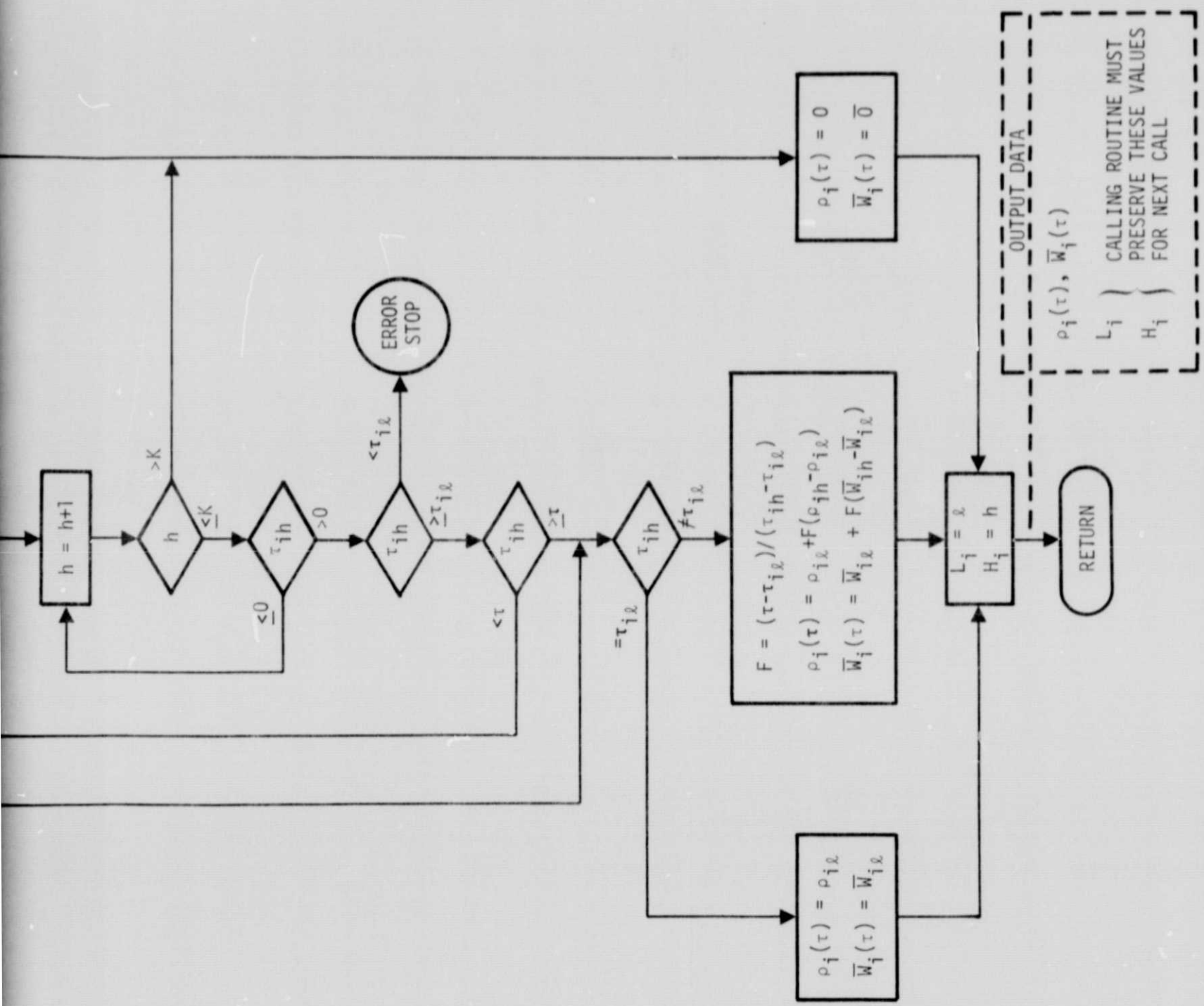


Figure 8. Flow Chart for Interpolation Subroutine

# REFERENCES

1. V. R. Wilmarth, "IUS/SSUS $Al_2O_3$ Plume Impingement Model," NASA/JSC Memorandum No. SC4-77-533, 3 November 1977 (Rev. 10 November 1977).

2. B. G. Jackson, "Minutes of Meeting: IUS and SUSS Solid Rocket Motor Exhaust Plume Analyses," NASA/JSC Memorandum No. EX32/7712-186, 30 December 1977.